Pergamon

Int. J. Solids Structures Vol. 33, No. 12, pp. 1689–1707, 1996

0020-7683/96 $15.00 + .00

0020-7683(95)00120-4

ON PATTERNS OF DEFORMATION IN PHASE TRANSFORMATIONS AND LÜDERS BANDS

STEPHEN BEISSEL
Department of Civil Engineering, Northwestern University, Evanston, IL 60093, U.S.A.

and

TED BELYTSCHKO
Departments of Civil and Mechanical/Nuclear Engineering, Northwestern University, Evanston, IL 60093, U.S.A.

(*Received* 11 *October* 1994; *in revised form* 18 *May* 1995)

Abstract—Materials which contain an unstable portion in the stress–strain relation frequently exhibit patterns of deformation characterized by alternating bands of large and small deformations. Certain metals produce these deformations as they undergo plastic straining or phase transformations. A rate-dependent material law including a field of imperfections is employed in a finite element model to produce a pattern of large and small deformations which resembles those observed experimentally. An essential feature of the formulation is the inclusion of a softening branch to the stress–strain curve to trigger the localization of strains, followed by a hardening branch to arrest it.

1. INTRODUCTION

Elastic–plastic materials and materials which undergo phase transformations often exhibit very distinctive patterns of deformations consisting of alternating bands. In adjacent bands, the material is in markedly different states of deformation. We have not seen any computations of the response of these materials which replicate these bands in any detail. The closest replication of a band-like structure has been by Collins and Luskin (1988), who showed a pattern of alternating deformation modes in a mesh of quadrilateral elements; however, the frequency of alternation coincided with the element size, which evokes the question of whether the phenomenon they observed was related to the discretization.

Silling (1988) has reported several interesting calculations of materials with phase changes around crack tips by means of dynamic relaxation. A salient feature of his computations was the lack of uniqueness in the results.

We have also found that in very homogeneous problems, the presence of an unstable branch in the stress–strain curve in a rate-independent material results in very chaotic results: the different phases are scattered almost randomly through the mesh. This is not surprising in view of results of Abeyaratne and Knowles (1991) that an infinite number of solutions exist in certain load states for such materials. However, when viscous regularization is used in the material model, the behavior becomes less chaotic (we are not speaking of chaos in the mathematical sense here). Nevertheless, the band-like patterns of deformation which are widely observed cannot be replicated.

It is shown here that when a pattern of imperfections is introduced into a material which contains softening and rehardening, the banded structure emerges clearly as the model is deformed. In fact, one can observe patterns of band growth such as are observed experimentally.

The common characteristic in certain elastic–plastic materials and phase changes which underlies the formation of these patterns is the presence of a portion of the stress–strain

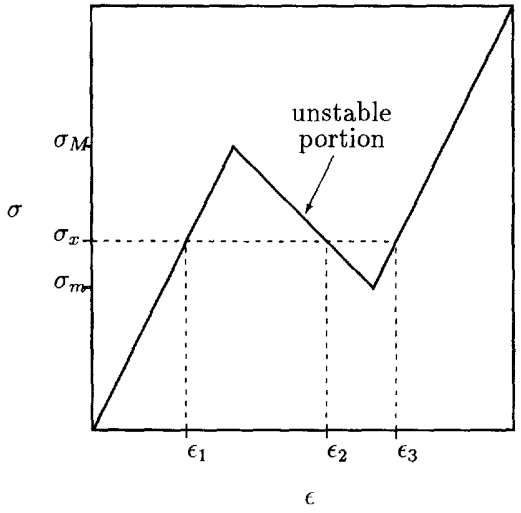

Fig. 1. Elastic stress–strain law with phase transitions.

response of the material where the stress decreases with increasing strain, as shown in Fig. 1. In this portion of the stress–strain curve, the material behavior is unstable in the sense of Hadamard (1903) and Hill (1962). The need for regularization of a rate-independent unstable material can be illustrated by a static bar subjected to end traction t. If t lies between σ_m and σ_M in Fig. 1, then there are three possible values of strain—ε_1, ε_2, ε_3—for every point.

Bazant and Belytschko (1985) showed that for rate-independent materials with an unstable branch that falls to zero stress, the onset of unstable material is limited to a set of measure zero and results in infinite strains. Subsequently, Belytschko *et al* (1987) showed that in a rate-independent material, even a small unstable portion, when followed by a perfectly plastic response, results in infinite strains on a set of measure zero. Both of the above studies were limited to one-dimensional bars under dynamic response.

Needleman (1988) has shown that the viscoplastic models developed to model strain-rate effects and other characteristics of metals under dynamic loads provide a regularization of the unstable material response, which differs from Landau–Ginsburg regularization. Although the applicability of viscoplasticity to phase changes is not clear, the principal purpose of the calculations given here is to show the qualitative character of the response.

2. FORMULATION

2.1. *Elastoviscoplastic constitutive model*

We will use an additive decomposition of the rate-of-deformation tensor into elastic and plastic parts,

$$\mathbf{D} \equiv \tfrac{1}{2}(\mathbf{L}+\mathbf{L}^{\mathrm{T}}) = \mathbf{D}^{\mathrm{e}}+\mathbf{D}^{\mathrm{p}} \tag{1}$$

where $\mathbf{L}$ is the spatial velocity gradient, $\mathbf{L} = \mathbf{v}\overleftarrow{\nabla}$, and $\mathbf{D}$ is the rate-of-deformation tensor. This leads to the elastoviscoplastic constitutive equation

$$\overset{\nabla}{\boldsymbol{\sigma}} = \mathbf{C}:\mathbf{D}^{\mathrm{e}} = \mathbf{C}:(\mathbf{D}-\mathbf{D}^{\mathrm{p}}) \tag{2}$$

where $\overset{\nabla}{\sigma}$ is the co-rotational stress rate of the Cauchy stress tensor, and $\mathbf{C}$ is the material moduli tensor for isotropic elasticity. The viscoplastic rate-of-deformation $\mathbf{D}^{\mathrm{p}}$ is calculated by means of a von Mises flow model,

$$\mathbf{D}^{\mathrm{p}} = \dot{\bar{\gamma}} \frac{3\mathbf{s}}{2\bar{\sigma}} \tag{3}$$

where $\mathbf{s}$ is the deviatoric stress tensor,

$$\mathbf{s} \equiv \boldsymbol{\sigma} - \tfrac{1}{3}(\boldsymbol{\sigma} : \mathbf{I})\mathbf{I} \tag{4}$$

and $\bar{\sigma}$ is the effective stress,

$$\bar{\sigma}^2 = \tfrac{3}{2}\mathbf{s} : \mathbf{s}. \tag{5}$$

The effective plastic strain rate, $\dot{\bar{\gamma}}$, is given by a power law rate relation,

$$\dot{\bar{\gamma}} = \dot{a}\left[\frac{\bar{\sigma}}{g(\bar{\gamma})}\right]^{1/m} \tag{6}$$

which is supported by experimental evidence, Asaro (1983) and Klopp (1985), over a large range of strain rates for elastic–plastic response, but its applicability to phase changes is still a matter to be investigated. The hardness function $g(\bar{\gamma})$ depends on the accumulated effective plastic strain $\bar{\gamma}$,

$$\bar{\gamma} = \int_0^{(t)} \sqrt{\tfrac{2}{3}\mathbf{D}^{\mathrm{p}} : \mathbf{D}^{\mathrm{p}}}\, \mathrm{d}t \quad \text{or} \quad \mathrm{d}\bar{\gamma} = \sqrt{\tfrac{2}{3}\mathbf{D}^{\mathrm{p}} : \mathbf{D}^{\mathrm{p}}}\, \mathrm{d}t. \tag{7}$$

2.2. *Numerical procedure*

The weak form of the momentum equation provides the basis for the finite element discretization in space.

$$\int_\Omega \overrightarrow{\nabla}(\delta\mathbf{u}) : \boldsymbol{\sigma}\, \mathrm{d}\Omega + \int_\Omega \rho\delta\mathbf{u} \cdot \dot{\mathbf{v}}\, \mathrm{d}\Omega = \int_{\Gamma_t} \delta\mathbf{u} \cdot \bar{\mathbf{t}}\, \mathrm{d}\Gamma + \int_\Omega \delta\mathbf{u} \cdot \mathbf{b}\, \mathrm{d}\Omega \tag{8}$$

where $\delta\mathbf{u}$ is any function in the space of C^0 functions which disappear on the essential boundary Γ_u, Ω is the domain, Γ_t is the natural boundary, and $\mathbf{b}$ is the vector of body forces. This must be solved simultaneously with the elastoviscoplastic constitutive relation

$$\overset{\nabla}{\boldsymbol{\sigma}} = \dot{\boldsymbol{\sigma}} - \mathbf{W} \cdot \boldsymbol{\sigma} - \boldsymbol{\sigma} \cdot \mathbf{W}^{\mathrm{T}} = \mathbf{C} : \left\{\mathbf{D} - \dot{a}\left[\frac{\bar{\sigma}}{g(\bar{\gamma})}\right]^{1/m} \frac{3\mathbf{s}}{2\bar{\sigma}}\right\} \tag{9}$$

(discussed in the previous section). The boundary conditions are

$$\mathbf{u}(\mathbf{x}, t) = \bar{\mathbf{u}} \quad \text{on} \quad \Gamma_u \tag{10}$$

$$\mathbf{n} \cdot \boldsymbol{\sigma}(\mathbf{x}, t) = \bar{\mathbf{t}} \quad \text{on} \quad \Gamma_t. \tag{11}$$

To discretize eqn (8) by finite elements in space the domain Ω is divided into elements Ω_e, and $\delta\mathbf{u}$ and $\mathbf{u}$ are approximated on each element by the interpolants

$$\mathbf{u}_e(\mathbf{x}) \approx \mathbf{N}(\mathbf{X})\mathbf{d}_e(t) \tag{12}$$

$$\delta\mathbf{u}_e(\mathbf{x}) \approx \mathbf{N}(\mathbf{X})\delta\mathbf{d}_e(t). \tag{13}$$

Subscripted e's denote quantities defined on the element e. The boolean matrix $\mathbf{L}_e$ extracts

members from the vector of globally interpolated displacements and arranges them in the corresponding elemental vector

$$\mathbf{d}_e = \mathbf{L}_e \mathbf{d} \tag{14}$$

$$\delta\mathbf{d}_e = \mathbf{L}_e \delta\mathbf{d}. \tag{15}$$

Expressing the vectors and tensors of eqn (8) in matrix notation and substituting eqn (12), (13), (14) and (15), the semi-discrete equations of motion are obtained.

$$\mathbf{M}\ddot{\mathbf{d}} = \mathbf{f}_{ext} - \mathbf{f}_{int}(\boldsymbol{\sigma}), \tag{16}$$

$\mathbf{M}$ represents the global lumped mass matrix; $\mathbf{f}_{ext}$, the external force vector; and $\mathbf{f}_{int}$, the internal force vector. The choice of the explicit central difference approximation in time yields the fully discrete equations,

$$\mathbf{d}^{n+1} = 2\mathbf{d}^n - \mathbf{d}^{n-1} + (\Delta t)^2 \mathbf{M}^{-1}[\mathbf{f}^n_{ext} - \mathbf{f}^n_{int}(\boldsymbol{\sigma})] \tag{17}$$

which must be combined with a finite difference scheme in time of the constitutive equations, eqn (9). In eqn (17), a superscript n refers to the time at the end of the nth time-step, $n\Delta t$. The finite difference schemes reduce the system of differential equations to a system of algebraic equations, which may be solved by an appropriate algorithm. The form of the algebraic system however depends on the choice of the finite difference schemes, and there is generally some trade-off between the simplicity of the algebraic equations and the accuracy of the approximation. The central difference scheme has been chosen to approximate the momentum equation (producing an explicit algorithm).

It therefore remains to choose a scheme to discretize the elastoviscoplastic constitutive equation, eqn (9). To make this choice, an examination of the constitutive equation in the following form is instructive.

$$\dot{\boldsymbol{\sigma}} = \mathbf{W}\cdot\boldsymbol{\sigma} + \boldsymbol{\sigma}\cdot\mathbf{W}^T + \mathbf{C}:\mathbf{D} - \dot{a}\left[\frac{\bar{\sigma}}{g(\bar{\gamma})}\right]^{1/m} \frac{3\mathbf{C}:\mathbf{s}}{2\bar{\sigma}}. \tag{18}$$

The left side contains the only time derivative term to be approximated, $\dot{\boldsymbol{\sigma}}$ ($\dot{a}$ being an empirical parameter). Approximating $\dot{\boldsymbol{\sigma}}$ over the interval from $n\Delta t$ to $(n+1)\Delta t$ by $(\boldsymbol{\sigma}^{n+1} - \boldsymbol{\sigma}^n)/\Delta t$, the terms of the right side must then be evaluated at some point in the interval. This can be expressed by the superscript $(n+\theta)\Delta t$, where $0 \leqslant \theta \leqslant 1$.

$$\frac{\boldsymbol{\sigma}^{n+1} - \boldsymbol{\sigma}^n}{\Delta t} = \left\{\mathbf{W}\cdot\boldsymbol{\sigma} + \boldsymbol{\sigma}\cdot\mathbf{W}^T + \mathbf{C}:\mathbf{D} - \dot{a}\left[\frac{\bar{\sigma}}{g(\bar{\gamma})}\right]^{1/m} \frac{3\mathbf{C}:\mathbf{s}}{2\bar{\sigma}}\right\}^{(n+\theta)\Delta t}. \tag{19}$$

The values $\theta = 0, 1/2, 1$ correspond to forward, central and backward difference schemes, respectively. In general, the value of θ affects both the accuracy and computational effort of the resulting scheme.

We shall begin by considering accuracy. Terms which change at an increasingly rapid rate render the forward difference scheme much less accurate than the other two schemes. The nonlinear last term of the right side—which involves the viscoplastic strain rate—changes in such a manner in the unstable part of the material response, due to high values of the exponent. Thus the use of $\theta = 0$ for this term greatly compromises the accuracy of the scheme. The other terms of the right side are not as highly nonlinear as the last term, and therefore do not compromise accuracy so severely when they are evaluated at $\theta = 0$.

With regard to computational effort, any value of θ other than $\theta = 0$ produces a nonlinear equation in $\boldsymbol{\sigma}^{n+1}$. It is desirable to avoid this since solving nonlinear equations for $\boldsymbol{\sigma}^{n+1}$ for each element for each of the many time-steps required by an explicit scheme

becomes intractable. A solution which includes an estimate of the last term of the right side for $\theta \neq 0$, and which remains linear, would be an optimal compromise. Such a construction is possible by expanding this term about the time $n\Delta t$ in a Taylor series, and keeping only the linear part. Details of this formulation are given in Pierce, Shih, and Needleman (1982) (who refer to it as the tangent modulus method), along with numerical examples which demonstrate the need for $\theta > 0$. The resulting algorithm consists of (i) solving the explicit equations of motion for $\mathbf{d}^{n+1}$, (ii) updating $\bar{\gamma}$ according to the numerical integration of eqn (7), and then (iii) updating $\boldsymbol{\sigma}$ by the tangent modulus method.

3. NUMERICAL RESULTS

3.1. *One dimension*

To examine the behavior of the viscoplastic formulation with softening and reharden-ing, a study is made of a simple one-dimensional model on $x \in (0,1)$. It is deformed by the prescribed end displacements,

$$u(0,t) = 0 \tag{20}$$

$$u(1,t) = vt \tag{21}$$

where $v = 1.0$ m s^{-1}. The hardness function $g(\bar{\gamma}; x)$ can be subdivided into $g_0(\bar{\gamma})$, the part which describes the evolution with effective plastic strain $\bar{\gamma}$, and $g(0; x)$, the part containing the spatial variation. Spatial variations in $g(\bar{\gamma}; x)$ are used to represent the inhomogeneous behavior caused by thermal effects or material imperfections. In this example, a small variation is introduced, with a maximum of one half of one percent at $x = 0.50$, Fig. 2, so

$$g(\bar{\gamma}; x) = g_0(\bar{\gamma}) + g(0; x) = g_0(\bar{\gamma}) + \begin{cases} (1.00 - 0.01x)\tau & \text{for } x < 0.5 \\ (0.99 + 0.01x)\tau & \text{for } x \geqslant 0.5. \end{cases} \tag{22}$$

The values of the material parameters are not intended to reflect those of a specific material. The parameters characterizing the hardness function are defined in Fig. 3, which illustrates the three stages of response. The material parameters are: E (the elastic modulus) = 100 MPa, $\tau = 1$ MPa, $\bar{\gamma}_M = \tau/E = 0.01$, $\bar{\gamma}_m = 30\bar{\gamma}_M = 0.3$, $g_{,\bar{\gamma}I} = 25$ MPa, $g_{,\bar{\gamma}II} = -1$ MPa, $g_{,\bar{\gamma}III} = 2.5$ MPa (Fig. 3), $a = 0.002$, $m = 0.02$, and $\rho = 0.001$ kg m^{-3}. The initial conditions are intended to minimize inertial effects so that the deformations will primarily reflect the nature of the constitutive relation.

$$u(x,0) = 0 \tag{23}$$

$$v(x,0) = vx. \tag{24}$$

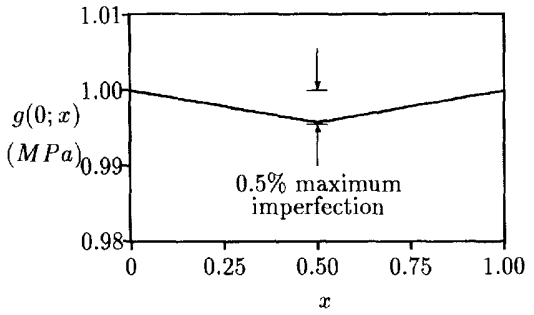

Fig. 2. Initial hardness function $g(0; x)$ displaying imperfection.

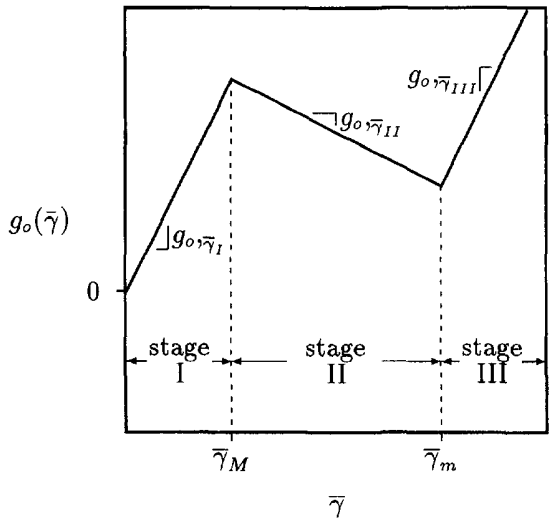

Fig. 3. Evolution of the hardness function with effective plastic strain.

Parameters of the numerical discretization are: $\theta = 0.5$, N (number of elements) = 49, $\Delta t = 1.0 \times 10^{-5}$ s; and the elements are linear.

Figure 4 is a plot of the total strain at successive points in time. Belytschko *et al* (1990) have demonstrated that the size of a band of localized strains depends on the size of the imperfection in the hardness function $g(\bar{\gamma}; x)$. Figure 4 shows clearly that when the material has passed stage I (which occurs at $\bar{\gamma} = \bar{\gamma}_M = 0.01$), the strains begin to localize at the center of the bar. To this point, the strains behave just as they would for a model which does not exhibit rehardening (stage III). Kulkarni and Belytschko (1991) performed a linearized perturbation analysis on the elastoviscoplastic equations of motion and showed that the condition for growth of a perturbation is that $g_{,\bar{\gamma}} < 0$. For the model under consideration, the perturbation takes the form of the imperfection in $g(\bar{\gamma}; x)$ and the condition for its growth, $g_{,\bar{\gamma}} < 0$, defines stage II. It has been demonstrated by Belytschko *et al* (1990) that the perturbation does not grow in an initial stage of hardening, where $g_{,\bar{\gamma}} > 0$, and it does not here. But the condition for the growth of a perturbation is also violated in stage III, and the localization which occurs in stage II cannot, therefore, continue when the material has entered the hardening zone of stage III. In Fig. 4, $\bar{\gamma}_m = 0.2$ and the numerical results show that the growth rate of the strains slows down when $\bar{\gamma}$ reaches $\bar{\gamma}_m$. The initial band of

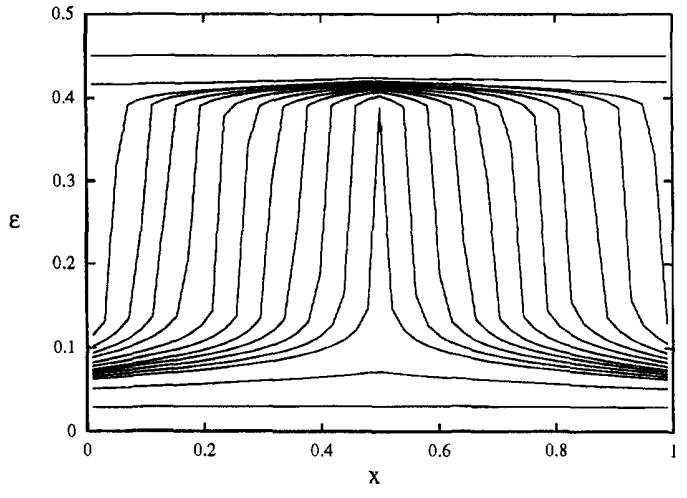

Fig. 4. Total strain distribution at successive points in time (plotting time increment = $3000\Delta t$).

high strain gradient then splits into two bands propagating like waves in opposite directions. In their wakes lies a virtually homogeneous region of strains where $\bar{\gamma} > \bar{\gamma}_m$, which replicates the behavior observed in Lüders deformations. The macroscopic manifestation of this behavior is an apparent "delocalization" of strains. When the waves reach the ends of the bar, the entire domain again becomes homogeneous and remains as such for the duration of the deformation. Although the imperfection remains in the hardness function, its influence on the strain distribution is quite minor after the entire bar reaches the rehardening stage. The pattern of deformation is also characteristic of a material whose stress–strain relation contains an unstable portion due to a phase transformation.

Figure 5a is a plot of the stress versus total strain in the center element of the bar. The initial sharply increasing segment is dominated by elastic deformation, as evidenced by the equality of its slope and the elastic modulus. The next segment, characterized by a smooth mild negative slope, reflects plastic deformations and is separated from the elastic segment by a peak in the stress. This segment corresponds to the softening portion (stage II) of the hardness function, and is completed before any element reaches stage III. In the final segment, associated with rehardening, unloading temporarily occurs in every element and the element which is softening causes the stress to drop in the entire mesh. The element in the softening range must then reach the hardening part of its stress–strain relation, causing the stress to increase in the entire mesh, before the next element can soften. Then when the next element does soften, the stress drops and the cycle is repeated. Elements which are equidistant from the center element go through softening and rehardening simultaneously, as the waves in Fig. 4 move toward the ends of the bar. The final effect is a series of unloading-and-reloading cusps. For the element at the middle of the bar, element 25 (Fig. 5a), all the cusps occur in stage III, since all other elements soften and reharden after it does. For element 13 (Fig. 5b) half of the cusps occur in stage II and half in stage III, since half of the elements soften and reharden before it, and half after. For the element at the left end of the bar, element 1 (Fig. 5c), all the cusps occur in phase II because all the other elements soften and reharden before it does. The portion of the plot in Fig. 5b between the two bundles of cusps is in fact a cusp itself, elongated by the large strains of the softening and rehardening process occurring in that element.

Multiple imperfections can be represented by a hardness function which contains several minima, Fig. 6. The next example illustrates the effects of such a model on the deformation process. The material properties, loading conditions, and initial conditions are the same as in the previous example, except that the initial hardness function, $g(0; x)$, now takes the form in Fig. 6. The evolution of the strain distribution is shown in Fig. 7. It can be seen that localization is triggered by each of the minima in the hardness function. As the deformation progresses, the maximum plastic strains exceed the limit of the softening stage, $\bar{\gamma} > \bar{\gamma}_m$, and their rates then decrease to near zero. Delocalization subsequently occurs as the waves of large strain gradient move away from the points of localization. When waves traveling in opposite directions meet, the deformation becomes homogeneous again.

3.2. *Two dimensions*

The one-dimensional model of the previous section served to demonstrate the basic evolution of deformation produced in a material with imperfections and a stress–strain relation containing an unstable portion. In two dimensions, the transition region between zones of high and low strains takes the form of a band. The development and subsequent motion of these bands are influenced by the fields of stress and imperfections.

Ananthan and Hall (1991), Hall (1970) and Nadai (1950) have documented for various alloys that tension tests generate Lüders bands at approximately 45° to the tensile axis, and the resulting deformations are predominantly shear strains. Thus the crucial stress in the initiation and development of the bands is that of shear. Also, it is demonstrated by Ananthan and Hall (1991) that the bands form in straight lines, with insignificant deviations at the grain boundaries. This implies that although the grain structure may influence the initiation of the bands (such as determining the exact location, or whether the angle will differ slightly from 45°), the morphology of the bands is driven by compatibility. The following plane strain examples illustrate the ability of the current formulation to reproduce

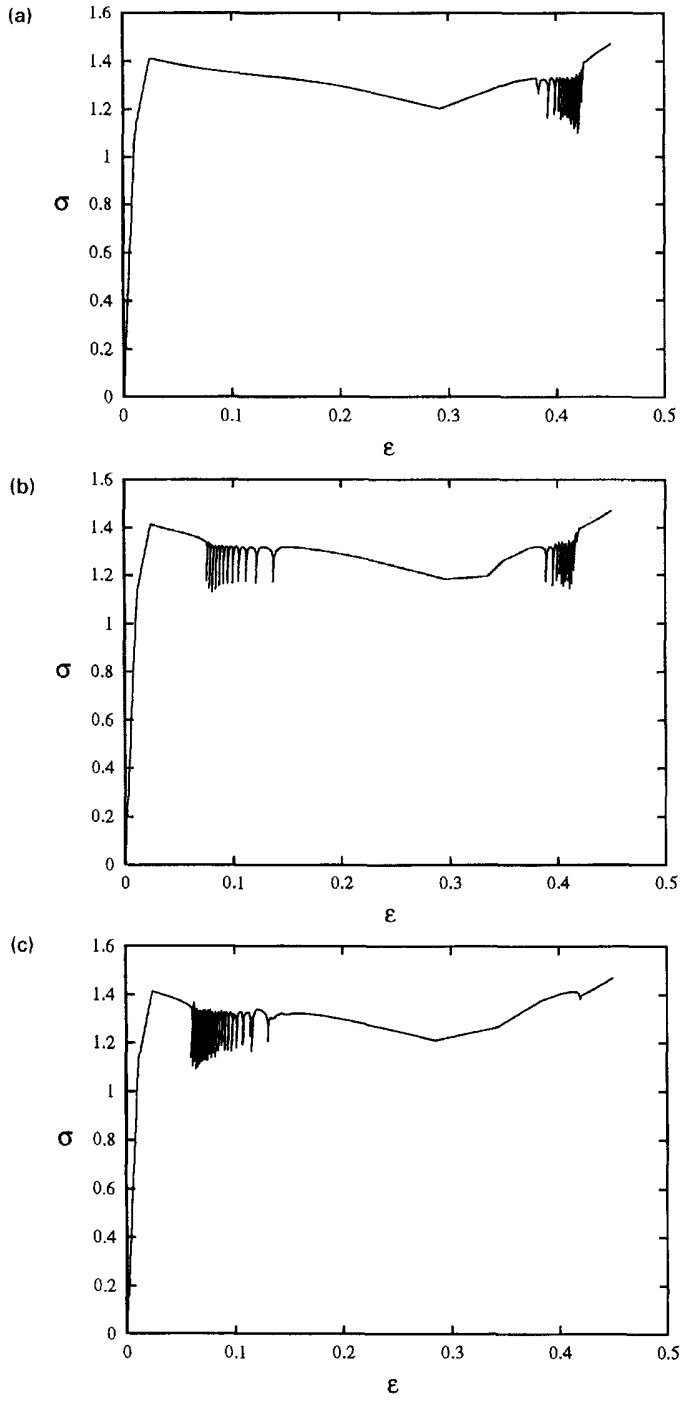

Fig. 5. Stress–strain plots at element: (a) 25; (b) 13; and (c) 1.

these observed features. Material model parameters for all the examples were the same and chosen as those typical of mild steels: $E = 211$ GPa, $\nu = 0.3$, $\dot{a} = 0.002$ s^{-1}, $m = 0.01$, $\tau = 460$ MPa, and $\rho = 7.8$ g cm^{-3}.

In the first example, we show that a moderate isolated imperfection results in a single band, and how rehardening affects its growth. A bar is subjected to prescribed displacements at each end. Twofold symmetry allows the modeling of only one quadrant; see Fig. 8. In the problem, the nodes at the left boundary of the mesh are fixed in the x-direction, those

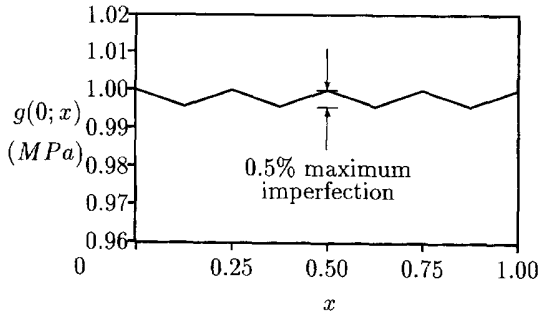

Fig. 6. Initial hardness function $g(0; x)$ displaying multiple imperfections.

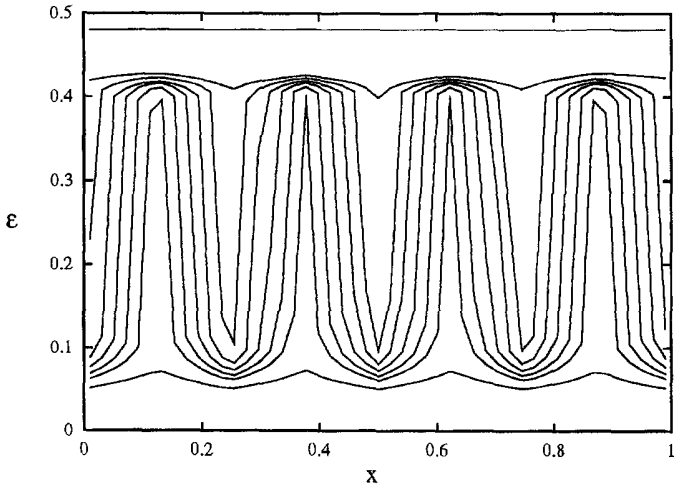

Fig. 7. Total strain distribution at successive points in time (plotting time increment = $6000\Delta t$).

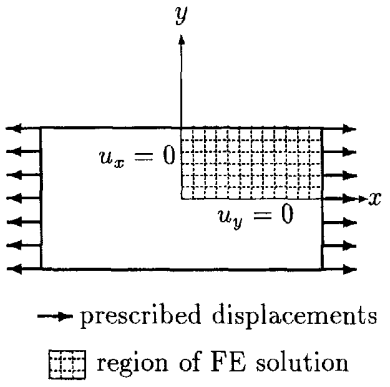

Fig. 8. Elongation of a bar.

at the right boundary are displaced in the x-direction. Free movement in the y-direction is allowed for all nodes but those on the bottom boundary, including those at the right and left boundaries. This arrangement is designed to model the elongation of a segment of a tension specimen which is far enough from the grips of the testing machine to avoid any transverse stresses caused by them, thus allowing the development of a homogeneous, tensile stress field.

The hardness function includes a small imperfection centered in the middle of the bar; $x = y = 0$ in Fig. 8,

$$g(\bar{\gamma}; x, y) = g_0(\bar{\gamma}) + g(0; r) = g_0(\bar{\gamma}) + \tau[1.00 - 0.01\, e^{(-r/r_0)}] \tag{25}$$

in which $r = \sqrt{x^2 + y^2}$ and scaling factor $r_0 = 0.000543$. The maximum imperfection is one percent of the undisturbed field. The dependence of the hardness function on the effective viscoplastic strain is contained in $g_0(\bar{\gamma})$, which is characterized by the parameters $\bar{\gamma}_M = 0.01$, $\bar{\gamma}_m = 0.1$, $g_{,\bar{\gamma}I} = 2800$ MPa, $g_{,\bar{\gamma}II} = g_{,\bar{\gamma}I}/4$, and $g_{,\bar{\gamma}III} = g_{,\bar{\gamma}I}$ (as defined in Fig. 3 for the undisturbed field of the one-dimensional example). Constant velocities are prescribed: $u_x = vt$, where $v = 4.0$ m s^{-1}. The body is initially at rest. The numerical discretization of the 0.004 by 0.0025 m domain is achieved by a mesh of 40 by 25 square, four-node quadrilateral elements. One point integration is employed with perturbation stabilization, Flanagan and Belytschko (1981), and a time-step of 2.0×10^{-5} s and a tangent modulus parameter $\theta = 0.50$.

Figure 9 shows plots of the effective plastic strain $\bar{\gamma}$ after 20,000 time-steps, demonstrating the localization of plastic strains in a band approximately 45° to the tensile axis. (Meshes with elements of different aspect ratios produce a band at the same angle.) At this stage in the deformation, the maximum effective strains are just reaching the softening limit and the effects of rehardening have not yet been realized. The significance of this configuration is the development of the band of large plastic shear strains, (i) from boundary and loading conditions which produce a uniform field of tensile stresses, and (ii) when the inhomogeneity is identical in all directions emanating from its center. This feature of the deformation has previously been reproduced numerically by Needleman (1989) and Belytschko *et al.* (1994) with softening viscoplastic models. Their models did not contain rehardening; continued loading, therefore, results in continued localization of shear strains in the band. Experiments in the quasi-static loading regime [e.g. Ananthan and Hall (1991)] for mild steels, indicate, however, that continued loading causes the band to split into two separating interfaces—as described in the one-dimensional results—leaving a region of nearly uniform, large plastic strains. This delocalization accommodates the prescribed displacements in a manner quite different from that of continued localization. It should be mentioned that loading rates of these computations, chosen to reduce inertial effects, model closely the testing conditions under which real experiments demonstrate delocalization. For the same materials under highly dynamic conditions, thermal softening cancels the effect of rehardening, and localization continues to material failure. The results of Needleman (1989) and Belytschko *et al.* (1994) model the dynamic experiments [see, for example, Marchand and Duffy (1988)].

Figure 10 shows the effective plastic strain distribution after continued loading to 32,000 time-steps. The contours show that the waves have separated and the resulting plastic strain field between them is nearly homogeneous and somewhat greater than the upper limit of the stage II strains. Thus, the delocalization exhibited in the one-dimensional example is manifest in two dimensions as the separation of two bands of high shear strain gradient at 45° to the tensile field—consistent with experimental results.

The purpose of the next example is to show that a two-dimensional structure of imperfections will result in a pattern of bands which resembles patterns often formed by Lüders bands and phase transformations. It also illustrates the observation that the morphology of Lüders bands is determined by compatibility of strains, not by the material grain structure. Figure 11 shows the 0.005 m square block which is subjected to pure shear, and the region of the finite element solution. In order to simulate the slight inhomogeneities caused by the granular structure of metals, the hardness function includes small variations in each direction. Figure 12 is a plot of the initial hardness function, which is given by,

$$g(\bar{\gamma}; x, y) = g_0(\bar{\gamma}) + \tau\left[1.00 + 0.01 \cos\left(\frac{6\pi x}{d}\right) + 0.009 \cos\left(\frac{6\pi y}{d}\right)\right] \tag{26}$$

where d = width of the model specimen = 0.0025 m and $g_0(\bar{\gamma})$ is the undisturbed field. The imperfections are not identical in both directions (1.0% in the x-direction and 0.9% in the y-direction) in order to simulate the slightly anisotropic character of the real imperfections

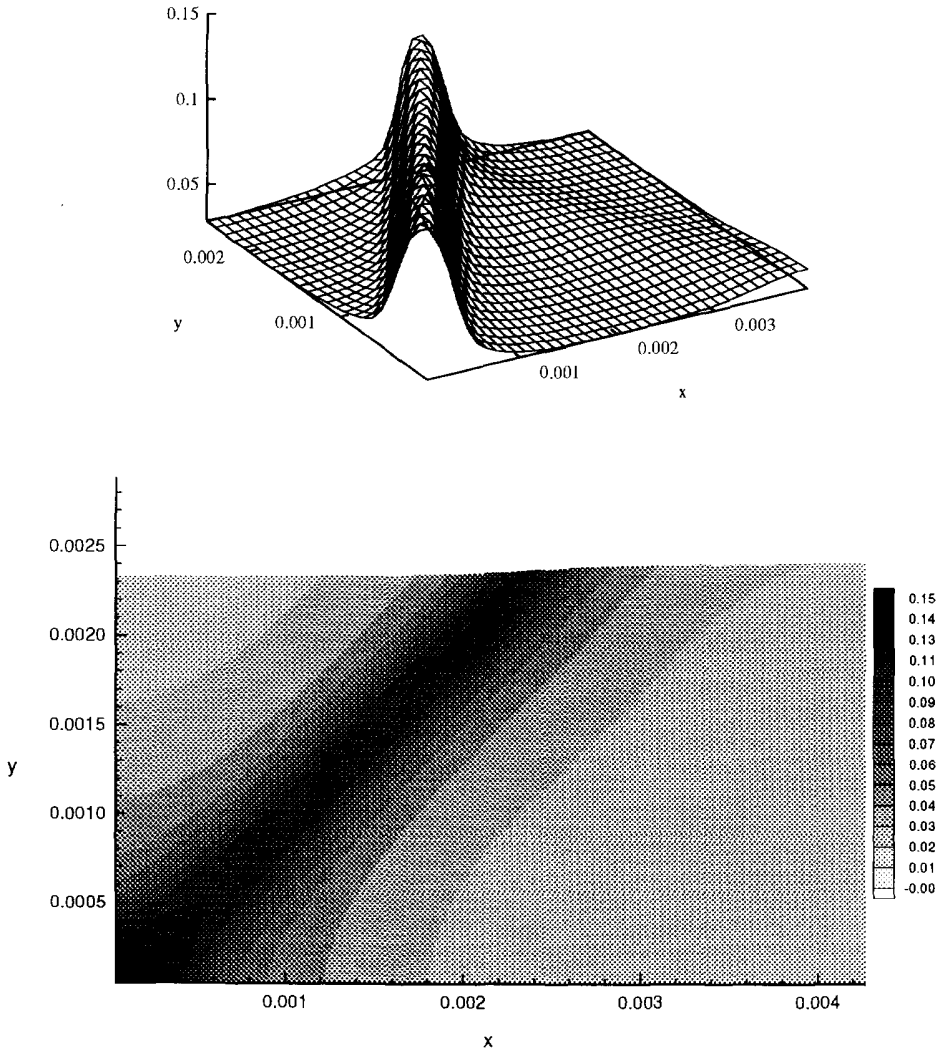

Fig. 9. Effective plastic strain distribution after 20,000 steps.

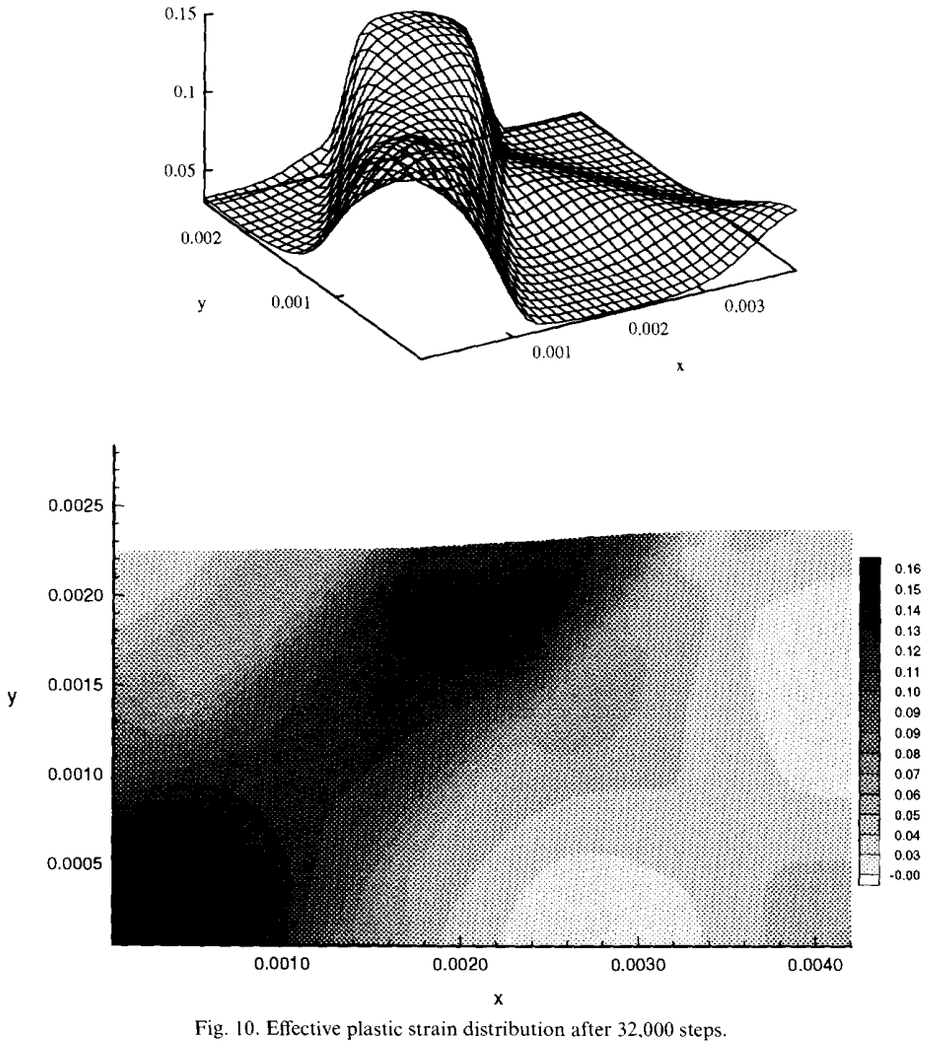

Fig. 10. Effective plastic strain distribution after 32,000 steps.

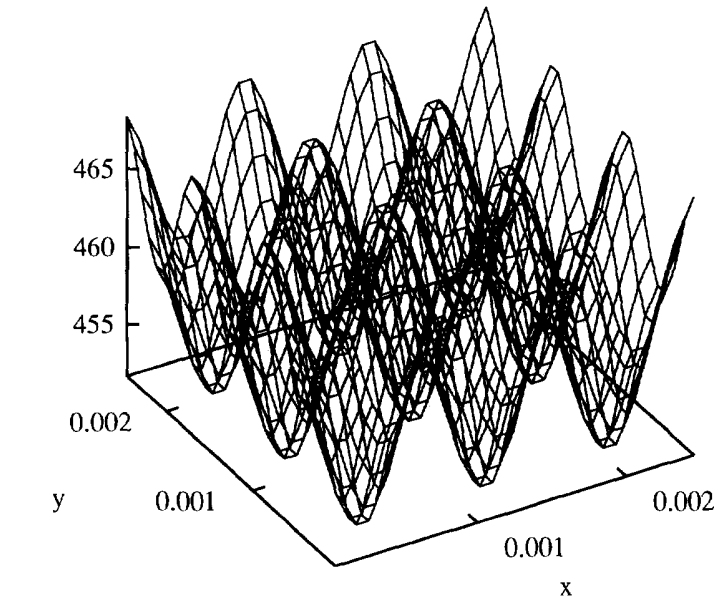

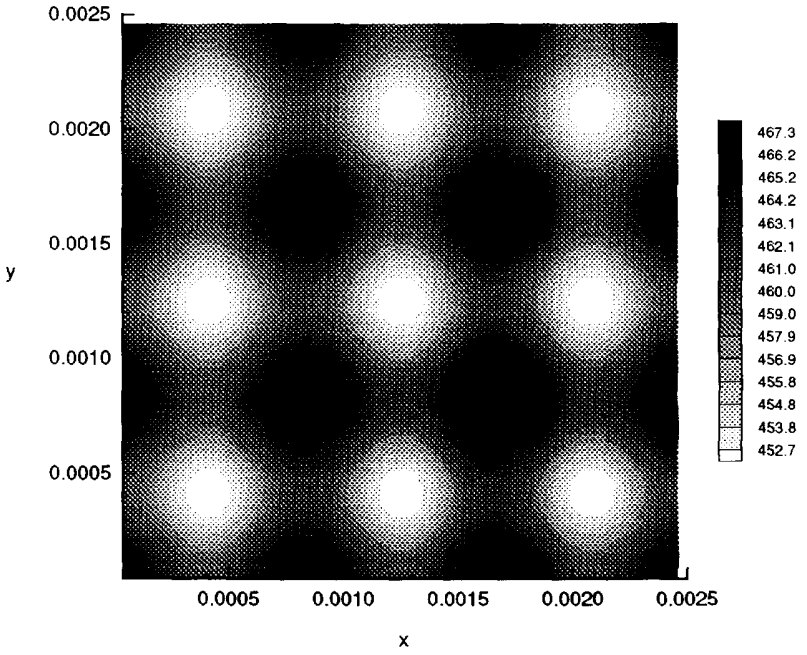

Fig. 12. Initial hardness function $g(0, x, y)$.

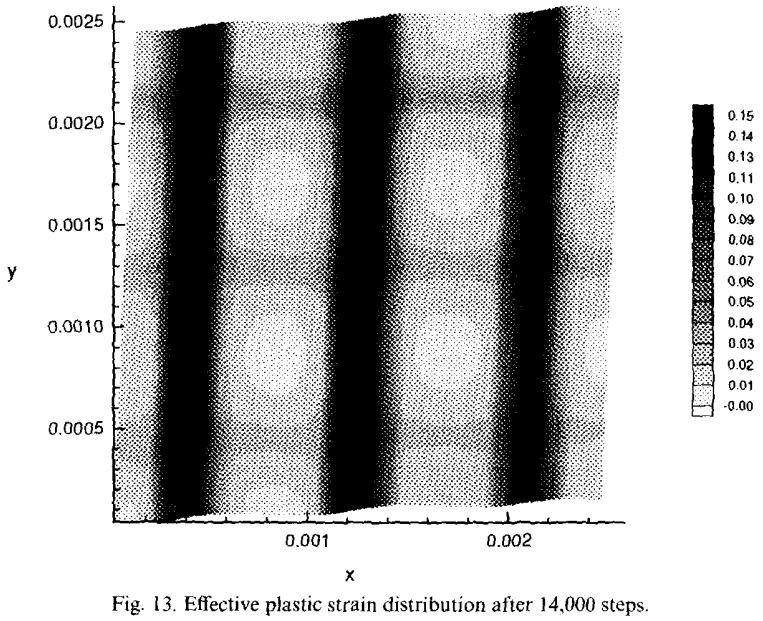

Fig. 13. Effective plastic strain distribution after 14,000 steps.

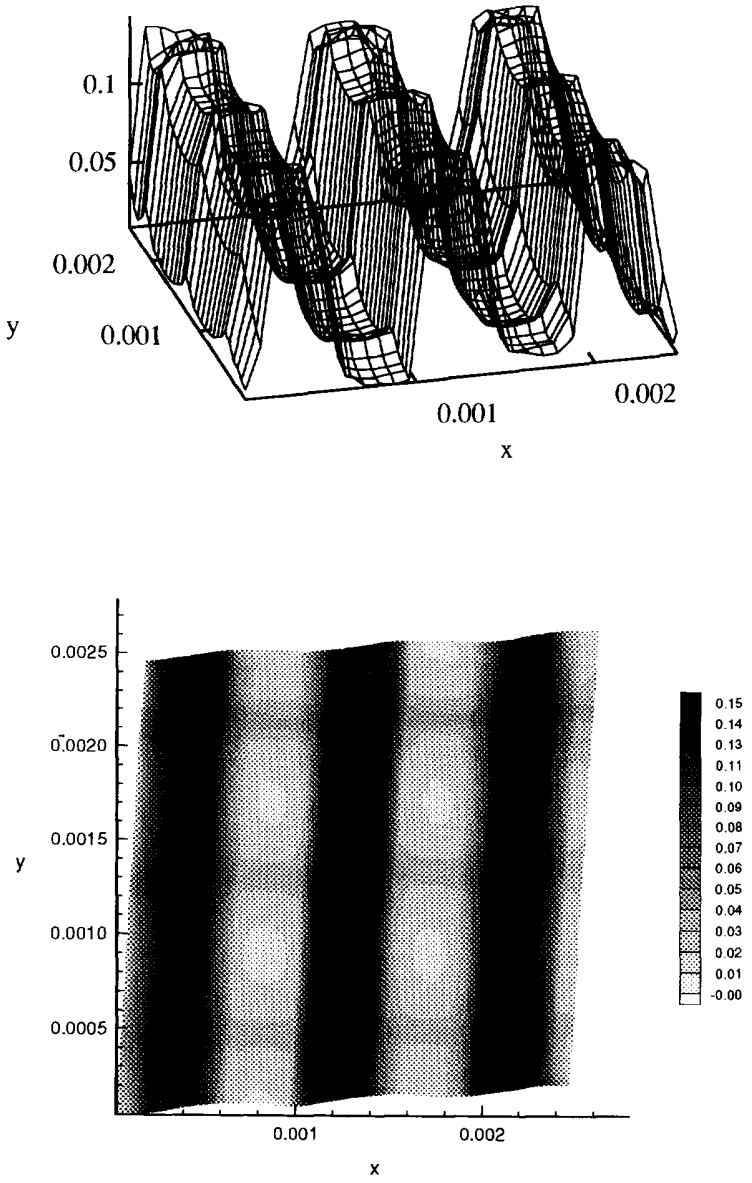

Fig. 14. Effective plastic strain distribution after 20,000 steps.

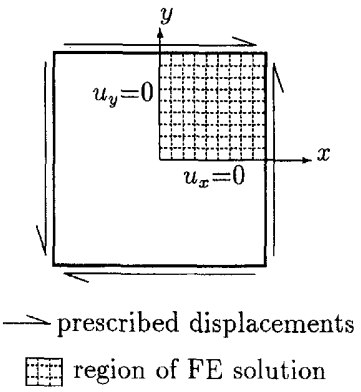

Fig. 11. Pure shearing of a square block.

in any material. A specimen of coarse-grained steel this size will likely exhibit this difference to a greater extent since the crystal grains are anisotropic and their size (several grains per mm) is significant compared to the specimen size. All the model parameters, the loading rate, and all the discretization parameters are identical to those of the previous example, with the exception of the mesh, which is 30 by 30 elements.

Figure 13 is a plot of the effective plastic strains after 14,000 time-steps. It reveals the formation of six bands of high strain gradient which have evolved from three parallel bands of localization. The regions between the bands alternate between small strains (light shading) and large plastic strains (dark shading), thus simulating the development of multiple Lüders bands—a phenomenon often observed in experimental results, even in those of simple tensile specimens [see Hall (1970)]. Figure 14 is a plot of the effective plastic strains after 20,000 time-steps, and Fig. 15 is the corresponding deformed mesh. The contours in Fig. 14 show that a field of parallel bands of high strains has evolved from an initial state of nearly homogeneous grain structure, as represented by the imperfections in the hardness function, Fig. 12. The reasons for this development are that the specimen is not perfectly identical in both directions—as any real specimen is not—and the material

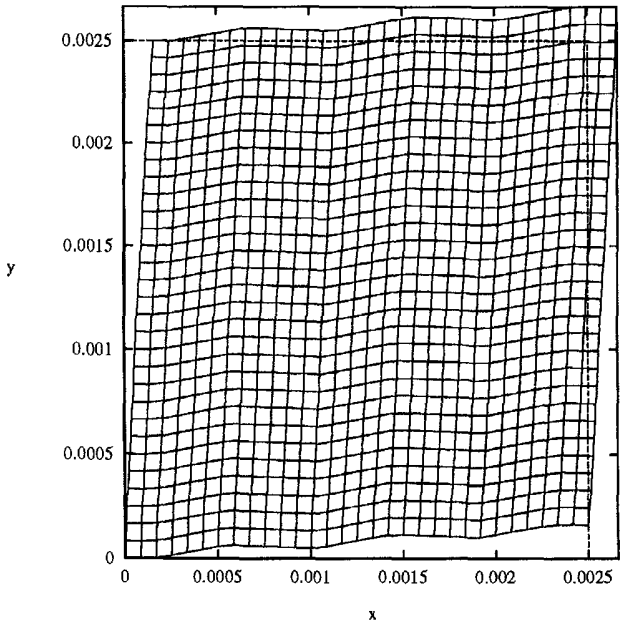

Fig. 15. Deformed mesh after 20,000 steps.

response includes softening. Both conditions are necessary: if the specimen imperfections were identical in both directions and the material unstable, identical bands of deformation would form in both directions; and if the material were stable but the specimen not identical in both directions, localizations would not occur and no bands would form. Once localization begins in the softening regime, it is the requirement that the strains produce deformations which are compatible with those prescribed at the boundaries, which drives the deformation into the banded structure.

Comparison of Fig. 14 to Fig. 13 illustrates the movement of the bands of high strain gradient away from the lines of localization, increasing the regions of large strains and decreasing the regions of small strains. This is the two-dimensional analogue of the process of delocalization depicted in Fig. 7.

4. CONCLUSIONS

It has been shown through computational studies that in the presence of imperfections, unstable material models can lead to band-like patterns of deformation such as are observed in Lüders bands and phase transformations. In the simulations, the equations of motion were solved with an explicit scheme, but the loads are applied quite slowly so that dynamic effects are minor. A viscoplastic model was used to avoid the difficulties associated with unstable material models.

The constitutive parameters for this model would be difficult to measure in the strain-softening range because in the strain-softening response a specimen will generally not remain homogeneous. Alternatives to this constitutive model are more fundamental approaches based on dislocation models with dislocation multiplication and annihilation, but these are still quite computationally intensive and were therefore not used. Nevertheless, the model qualitatively shows patterns of deformation similar to those observed in experiments.

The two-dimensional calculation was the more interesting. It showed that in the presence of a complex pattern of imperfections of very small magnitude (about one percent) in the strength of the material, band-like patterns of deformation emerge as long as the imperfection has a slightly stronger amplitude in one direction. Furthermore the size of the bands depends on the scale of the imperfections. Since imperfections are always present in real materials, this suggests that the widths of the bands in unstable response represent the scale of dominant imperfections. In the problems studied here, the bands aligned with the direction of the stronger imperfection. We have attempted to obtain two sets of bands which are orthogonal to one another and contained in separate regions of the same specimen, as are often observed, but were not successful.

Acknowledgements—The support of the National Science Foundation and the Air Force Office of Scientific Research is greatfully acknowledged.

REFERENCES

Abeyaratne, R. and Knowles, J. K. (1991). Kinetic relations and the propagation of phase boundaries in solids. *Arch. Rational Mech. Anal.* **114,** 119–154.

Ananthan, V. S. and Hall, E. O. (1991). Macroscopic aspects of Lüders band deformations in mild steel. *Acta Metall. Mater.* **39(12),** 3153–3160.

Asaro, R. J. (1983). Mechanics of crystals and polycrystals. *Adv. Appl. Mech.* **23,** 2–115.

Bazant, Z. P. and Belytschko, T. (1985). Wave propagation in a strain-softening bar: exact solution. *J. Engng Mech.* **111(1),** 381–389.

Belytschko, T., Wang, X. J., Bazant, Z. P. and Hyun, Y. (1987). Transient solutions for one-dimensional problems with strain-softening. *J. Appl. Mech.* **54,** 513–518.

Belytschko, T., Moran, B. and Kulkarni, M. (1990). Stability and imperfections in quasistatic viscoplastic solutions. *Appl. Mech. Rev.* **43(5),** 251–256.

Belytschko, T., Chiang, H. Y. and Plaskacz, E. (1994). High resolution two dimensional shear band computations: imperfections and mesh dependence. *Comput. Methods Appl. Mech. Engng* **119,** 1–15.

Collins, C. and Luskin, M. (1988). The computation of the austenitic-martinsitic phase transition. *PDE's and Continuum Models of Phase transitions, Proceedings*. Springer-Verlag, Nice.

Flanagan, D. P. and Belytschko, T. (1981). A uniform strain hexahedron and quadrilateral and hourglass control. *Int. J. Numer. Methods Engng* **17,** 679–706.

Hadamard, J. J. (1903). *Leçons sur la Propagation des Ondes et les Equations de L'Hydrodynamic*. Libraire Scientifique A. Hermann, Paris.
Hall, E. O. (1970). *Yield Point Phenomena in Metals and Alloys*. Plenum Press, New York.
Hill, R. (1962). Acceleration waves in solids. *J. Mech. Phys. Solids* **10,** 1–16.
Klopp, R. W., Clifton, R. J. and Shawki, T. G. (1985). Pressure-shear impact and the dynamic viscoplastic response of metals. *Mech. Mater.* **4,** 375–385.
Kulkarni, M. and Belytschko, T. (1991). On the effect of imperfections and spatial gradient regularization in strain softening viscoplasticity. *Mech. Res. Commun.* **18,** 335–343.
Marchand, A. and Duffy, J. (1988). An experimental study of the formation process of adiabatic shear bands in a structural steel. *J. Mech. Phys. Solids* **36(3),** 251–283.
Nadai, A. (1950). *Theory of Flow and Fracture in Solids*, Vol. 1, Second Edition. McGraw-Hill, New York.
Needleman, A. (1988). Material rate dependence and mesh sensitivity in localization problems. *Comput. Methods Appl. Mech. Engng* **67,** 69–85.
Needleman, A. (1989). Dynamic shear band development in plane strain. *J. Appl. Mech.* **56,** 1–9.
Pierce, D., Shih, C. F., and Needleman, A. (1982). A tangent modulus method for rate-dependent solids. *Comput. Struct.* **18,** 875–886.
Silling, S. A. (1988). Numerical studies of loss of elipticity near singularities in an elastic material. *J. Elasticity* **19,** 312–239.